Advances in Water Resources 50 (2012) 31–40

Contents lists available at SciVerse ScienceDirect

Advances in Water Resources

journal homepage: www.elsevier.com/locate/advwatres

Soil heat flux variability influenced by row direction in irrigated cotton ☆

Nurit Agam [a,*], William P. Kustas [b], Steven R. Evett [c], Paul D. Colaizzi [c], Michael H. Cosh [b], Lynn G. McKee [b]

[a] Gilat Research Center, Agricultural Research Organization, Rural delivery Negev, 85280, Israel
[b] USDA-ARS, Conservation & Production Research Laboratory, P.O. Drawer 10, Bushland, TX 79012, USA
[c] USDA-ARS, Hydrology & Remote Sensing Lab, Bldg. 007, BARC-West, Beltsville, MD 20705, USA

ARTICLE INFO

Article history:
Available online 20 July 2012

Keywords:
Soil heat flux
Row direction
Row crop

ABSTRACT

Spatial and temporal variability in soil heat flux (G) under sparse/clumped vegetation conditions is significant and has been studied. However, little attention has been devoted to evaluating the variability of G with respect to row crops, particularly with respect to row direction. The variation in G for row crops is related to the effect of differential shading of the soil surface, which is dependent on plant architecture, row spacing, and row direction. This paper reports the effect of row direction and sensor position on G magnitude and variability in an irrigated row crop of cotton. In addition, the effect of errors in water content estimation on the heat storage in the uppermost soil layer is assessed. The research was conducted in the Southern High Plains of the USA, as part of the Bushland Evapotranspiration and Agricultural Remote Sensing Experiment of 2008 (BEAREX08). Measurements were concentrated in two irrigated cotton fields, one with north–south (N–S) and the other with east–west (E–W) row directions, with ten sets of sensors in each field. Row direction had an effect on both the temporal dynamics and the total daily G. Important short-term (15-min average) variability in G at the various positions in the interrow was observed under partial canopy cover conditions for the N–S row direction, while the daily sum of G (ΣG) in both row directions was similar. In the beginning and the end of the growing season, ΣG was larger in the N–S direction field. In the E-W direction field, strategically located 3-replicate sensor sets (as are often deployed at flux tower installations) were found to adequately describe the 10-sensor average G, with errors as small as 6% and with a transitory maximum error of 12%. In the N-S row direction field, however, no 3-position combination was adequate to represent the 10-sensor average G.

1. Introduction

In temperate humid climates, where 100% vegetation cover is common, soil heat flux (G) is a relatively small component of earth's surface energy balance [1–3]. Since micro-meteorological techniques for estimating surface fluxes were initially developed in temperate regions, G was not considered to be a critical component of the surface energy balance. However, under sparse vegetation conditions G may reach 50% of net radiation [4] and even for taller canopies, including forests, can account for 30–50% of net radiation [5,6]. Therefore, inaccurate estimates of G may lead to non-negligible errors in the surface energy balance [7]. Moreover, in all climates, tillage practices associated with cropping often leave soil surfaces bare as do some harvest practices, and in both cases G may again reach 50% of net radiation.

In situ estimates of G at the surface can be obtained with soil heat flux plate measurements summed with measurements of the change in heat storage in the soil layer above the plate, often termed the combination method. Heat flux plates are generally installed at 0.05–0.15 m below the surface [8]. In some cases, heat flux plates have been placed at more shallow depths of 0.01–0.02 m e.g., [9, 10] in order to reduce the uncertainty and errors associated with correcting for soil temperature and water content change above the plate. However, shallower placement may introduce much larger errors, compared to deeper deployment. The larger errors are associated with (i) differences in thermal conductivity between the plate and soil, which can cause the heat flux to diverge around the plate or to converge through the plate; and (ii) interference by the plate with soil water flux, which can cause soil water contents above and below the plate to diverge greatly from values attained in the surrounding field, in turn caus-

☆ The US Department of Agriculture (USDA) prohibits discrimination in all its programs and activities on the basis of race, color, national origin, age, disability, and where applicable, sex, marital status, familial status, parental status, religion, sexual orientation, genetic information, political beliefs, reprisal, or because all or part of an individual's income is derived from any public assistance program. (Not all prohibited bases apply to all programs.) Persons with disabilities who require alternative means for communication of program information (Braille, large print, audiotape, etc.) should contact USDA's TARGET Center at (202) 720-2600 (voice and TDD). To file a complaint of discrimination, write to USDA, Director, Office of Civil Rights, 1400 Independence Avenue, SW, Washington, DC 20250-9410, or call (800) 795-3272 (voice) or (202) 720-6382 (TDD). USDA is an equal opportunity provider and employer.

* Corresponding author. Tel.: +972 52 2292131; fax: +972 8 9926485.
E-mail addresses: agam@agri.gov.il, nurit.agam@gmail.com (N. Agam).

0309-1708/$ - see front matter © 2012 Elsevier Ltd. All rights reserved.
http://dx.doi.org/10.1016/j.advwatres.2012.07.017

ing both incorrect heat storage measurements in the soil above the plate and heat divergence or convergence. Indeed, significant errors in G were reported when heat flux plates were deployed shallower than 0.03 m (e.g., [11]).

A heat flux plate provides an estimate of G (G_z) at the depth at which it is deployed. The difference between G at the soil surface and G_z is due to the change in heat storage within the soil layer above the plate (ΔG_s), which can be accounted for by:

$$\Delta G_s = C_V(t)\frac{\partial T}{\partial t}dz \quad (1)$$

where dz is the thickness of the soil layer above the heat flux plate, $C_V(t)$ is the time dependent average volumetric heat capacity of the layer, and $\partial T/\partial t$ is the average time rate of change in soil temperature in this layer. By summation of G_z and ΔG_s the G at the soil surface is obtained [12,13]:

$$G = G_z + \Delta G_s \quad (2)$$

Prior to computing ΔG_s, the value of $C_V(t)$ must be assessed. Knowledge of the time-dependent volume fractions of mineral soil (θ_m), organic matter (θ_o), water (θ), and air (θ_a) allows the determination of C_v as [14]:

$$C_v(t) = \rho_m\theta_m(t)c_m + \rho_o\theta_o(t)c_o + \rho_w\theta(t)c_w + \rho_a\theta_a(t)c_a \quad (3)$$

where c_i denotes the specific heats and ρ_i denotes the densities.

In Eq. (3) the water content θ is the component undergoing the most noticeable temporal variations. Therefore, in order to accurately compute ΔG_s, continuous measurements of soil water content must accompany soil temperature measurements in the soil above a heat flux plate. In the early 1980s, several methods were developed to allow continuous long-term monitoring of θ. One method relies on measurements of soil electrical properties, including time domain reflectometry (TDR) (e.g., [15,16]). When carefully calibrated, TDR was found to accurately determine θ [17]. Another method is based on capacitance measurements. By analysis of the behavior of an oscillating resonant electromagnetic field in soil the capacitance is determined, from which the dielectric permittivity, and in turn θ may be estimated [18,19]. While capacitance methods are currently ubiquitous, several studies have questioned their accuracy and have detailed important interferences from soil bulk electrical conductivity and bound water as well as the temperature effects on both of these [20–23].

In addition to the effect of measurement accuracy on local estimation of G, the heterogeneous nature of plant cover must be accounted for if an area-average G is required, as is the case in energy balance studies. On uniform surfaces with near full vegetation cover, G can be estimated fairly reliably with three to five replicate sensor sets [3]. However, under sparse and/or clumped vegetation cover conditions, spatial variation in G can be significant [2,24–26]; and inadequate spatial sampling of G may contribute to the failure to close the surface energy budget [11,27–30]. There is uncertainty as to the number of soil heat flux sensors required to obtain a representative soil heat flux for most heterogeneous surfaces. For example, in forest and riparian environments it was reported that the number of soil heat flux replicates needed to provide sufficient sampling of G may exceed 20 [31]. Kustas et al. [3] tested the variability in G in a sparsely populated mesquite shrub site, and found that a five-sensor array arranged in an "X" pattern could determine G in good agreement with a 20-sensor array. The five-sensor array was arranged in the cardinal directions (southerly, northerly, easterly and westerly) to account for micro-topographic/shading effects with changing solar altitude and azimuth angles. However, when using other five-sensor array configurations, differences from the 20-sensor array were significantly larger and similar to those of a three-sensor array, indicating that site selection of a relatively small number of sensors is critical. They concluded that it would seem nearly impossible to provide a recommendation on the minimum number of sensors required for a reliable estimate of G for such a surface.

Obviously, there are practical limitations to the number of sensors one can use to obtain a representative value within several meters of a flux tower, especially when trying to obtain representative G values commensurate with the source-area footprint of flux sensors [3]. Care in sensor deployment is therefore necessary for accurate measurement in grasslands and other semi-arid to arid ecosystems where G is a significant fraction of the net radiation [26].

While some research has assessed the variability in G under sparse/clumped vegetation conditions [3,26], little has been done with respect to row crops with different row directions [2]. By its nature, cultivation of row crops leaves a large portion of the soil surface exposed throughout much of the growing season, during which differential shading of the surface, coupled with other microclimatic factors, influences the spatial variation of G beneath the canopy [25]. The effect of differential shading of the surface is dependent on plant architecture, row spacing, row direction, and sun azimuth and zenith angles. The main objective of this research was to study the effect of row direction on G magnitude and variability in an irrigated semi-arid agricultural area. In addition, the effect of incorrect water contents on calculation of ΔG_s was assessed.

2. Materials and methods

2.1. Site description

The research was conducted at the USDA-ARS Conservation & Production Research Laboratory, Bushland, Texas (35° 11′ N, 102° 06′ W, 1170 m above mean sea level), in the US Southern High Plains, as part of the Bushland Evapotranspiration and Agricultural Remote Sensing Experiment of 2008 (BEAREX08, [32]). Measurements were concentrated in two of four square 4.4-ha fields, each containing a large weighing lysimeter in its center, where irrigated cotton was planted on May 21, day of year (DOY) 142, 2008 in row spacing of 0.76 m. Row directions were north–south (N–S) and east–west (E–W) in the northeast (NE) and southeast (SE) fields, respectively. The soil is a Pullman series silty clay loam, a fine, mixed, superactive, thermic Torrertic Paleustoll, which had a bulk density of 1.1 Mg m^{-3}, porosity of 0.61 m^3 m^{-3} and mineral fraction of 0.39 m^3 m^{-3} at 5-cm depth. Organic matter content was 1% by mass. This is a common value for continuously tilled Pullman soil in the semi-arid climate at Bushland, despite its classification as a Mollisol.. The volume fraction of organic matter was considered negligible.

2.2. Measurements

To account for the spatial variability of G, two replicates of five positions across the interrow were used (Fig. 1), with sensor sets centered at distances of 0.075, 0.225, 0.375, 0.525, and 0.675 m from the row center. In each location, a soil heat flux plate (model HFT-3.1 heat flow transducer, Radiation and Energy Balance Systems, Inc. Bellevue, WA*) was installed at a depth of 80 mm. The HFT-3.1 transducer is circular with a nominal 40 mm diameter and 4 mm thickness and with a thermal conductivity of 1.22 W m^{-1} K^{-1}. A study of the performance of soil heat flux plates by Sauer et al. [33] indicated that the HFT design is robust. Thermocouples were in-

* Mention of trade names or commercial products in this article is solely for the purpose of providing specific information and does not imply recommendation or endorsement by the US Department of Agriculture.

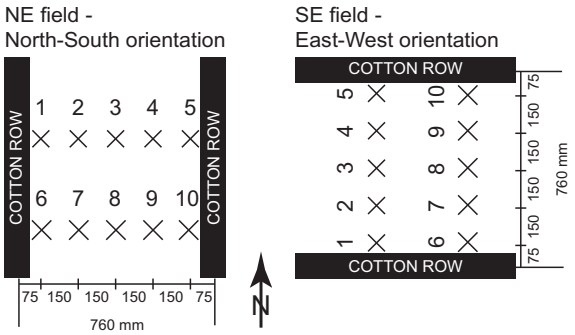

Fig. 1. Position within the interrow of sets of soil heat flux plates and thermocouples in both the NE (north–south row direction) and the SE (east-west direction) fields. TDR probes were deployed in the same position relative to the row, in the NE field only.

stalled above each plate at 60-, 20- and 0-mm depths. The sensors were sampled every 10 s and 15-min averages were stored on Campbell Scientific CR1000 data loggers.

In the NE field, θ was determined using soil-specifically calibrated [17] conventional TDR probes (θ_{TDR}) [34] inserted horizontally into the side of a soil pit, at 20 and 60 mm depths above each heat flux plate (total of 20 TDR probes). After insertion, the pit was backfilled. TDR measurements were not made in the SE field. In addition, six (in the NE field) and five (in the SE field) dielectric permittivity sensors (Hydra Probe, Stevens Water Monitoring Systems, Inc., Portland, OR, USA) [35] were horizontally installed, centered at 5-cm depth and sensing θ across a depth of 3–7 cm approximately. Four (in the NE field) and three (in the SE field) of the Hydra Probe (HP) sensors, that were located reasonably close to the G measurement sites, were averaged to determine the HP volumetric water content (θ_{HP}) (for more details on the spatial distribution of the HP sensors see [36]). Plant height and width were measured periodically in three replicates in each field, and a fractional vegetation cover (f_c) was estimated.

Net radiation (R_n) was measured in proximity to the G arrays using four-component net radiometers (CNR-1, Kipp and Zonen, Delft, The Netherlands). An intercomparison study of several four-component net radiometers, excluding the two used here, was conducted prior to the beginning of the experiment. This study indicated that these measurements have an uncertainty of approximately 12 W m^{-2} [37].

2.3. Soil water sensor calibrations

The TDR system was specifically calibrated for the Pullman soil, using mass balance methods, resulting in an accuracy of

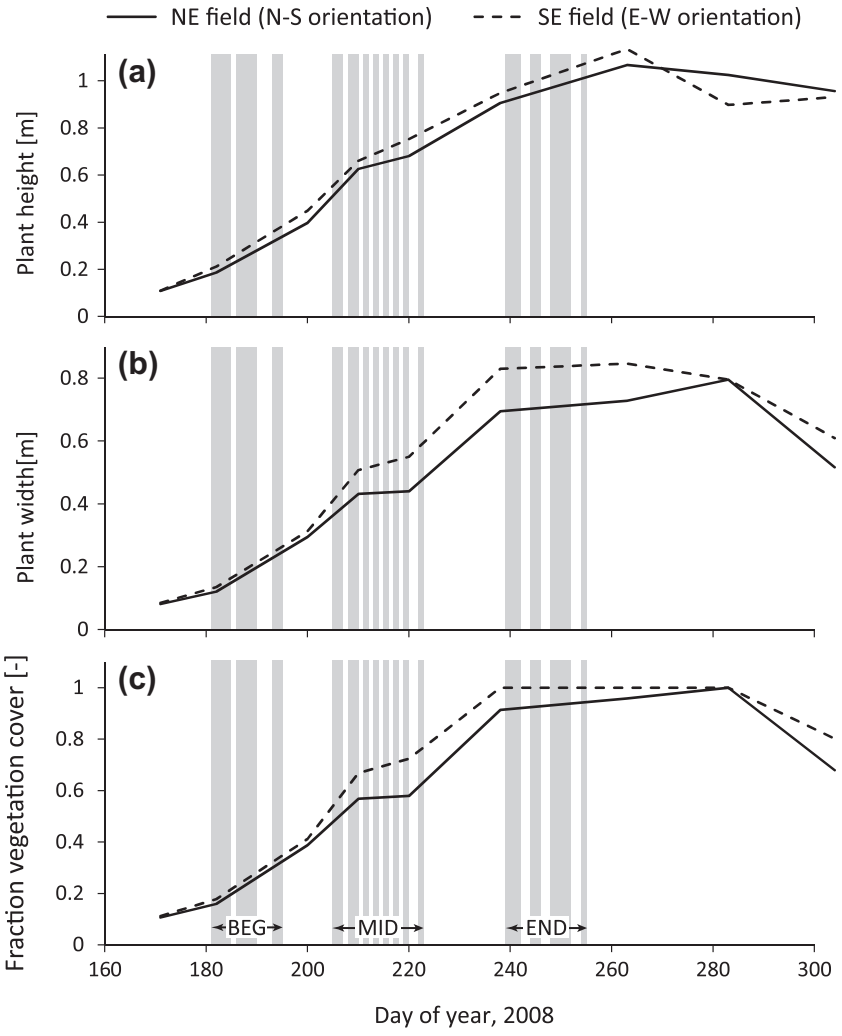

Fig. 2. Plant height (a), plant width (b), and fractional vegetation cover (c) during the cotton's growing season, 2008, in both the NE and SE fields (north-south and east-west row directions, respectively). The gray bars indicate the days from which data were used to calculate an "average" day for the beginning (BEG), middle (MID) and end (END) sub-periods.

$\leqslant 0.01\ m^3\ m^{-3}$ [17]. The HP sensors have four factory calibration polynomial curves [15,39] depending on the texture of the soil (sand, silt, clay, and loam) [38]. For the Pullman soil, the "Loam/general" calibration curve resulted in the best estimates of water content compared with calibrated TDR data [17], but still overestimated permittivity, thus requiring a soil-specific calibration [21].

Soil specific calibration of the HP sensors was performed by comparison to TDR readings and was applied in two steps. First, six TDR probes and six HP sensors were deployed in close proximity so that they all experienced the same changes in water content, temperature and bulk electrical conductivity. A linear regression between HP real permittivity values and apparent permittivity values determined with the TDR system was performed ($r^2 = 0.97$, RMSE = 1.1 $m^3\ m^{-3}$) and the HP real permittivity values were corrected by $x = (y + 1.54)/1.437$ where x is the corrected value and y is the real permittivity value output by the HP [21]. Second, corrected HP water contents (θ_{HP_C}) were computed using the soil-specific calibration for the TDR system $\theta = -0.146 + 0.1095(permittivity)^{0.5}$ [17]. This correction procedure for the HP data was used by Cosh et al. [36] in generating water content estimates from the network of sensors deployed in the field.

2.4. Soil heat flux computation

Soil heat flux was computed separately for each of the 10 locations in each field, based on Eq. (2). The value of $C_v(t)$ was computed following Eq. (3), with the specific form [14]:

$$C_v(t) = [1.94\theta_m + 2.5\theta_o + 4.19\theta(t)] \cdot 10^6 \quad (4)$$

where θ_m and θ_o were considered time invariant. For the NE site, computation of ΔG_s with Eq. (1) was repeated three times – using θ_{TDR}, θ_{HP}, and θ_{HP_C}. When computing ΔG_s with θ_{TDR}, since both temperature and θ measurements were available at both 20 and 60 mm depths, the soil layer above the G_P was divided into two layers: 0–40 and 40–80 mm, and the heat storage change term was computed for each layer separately. The total value of ΔG_s was then taken as the sum of storage change of the two layers. For the two other cases (using corrected and uncorrected HP data), and since there was only one HP θ value for the 0-80 mm layer, ΔG_s was computed using average temperature of the layer (averaging data from thermocouples at 20 and 60 mm). For the SE field, ΔG_s was computed using θ_{HP_C} only. Each positional G (for positions 1–5, $G_{1\text{-}5}$) was determined as the average of the two repetitions (i.e., sensors 1 and 6 for position 1, 2 and 7 for position 2 etc., see Fig. 1). The flux sign convention used in the current study is fluxes away from the soil surface are positive.

2.5. 3 sub-periods

Data were collected throughout the growing season, and three sub-periods representing the beginning (BEG), middle (MID), and end (END) of the growing season were defined, based on plant height and width, and fractional vegetation cover (Fig. 2). In each sub-period, 10 days meeting the following criteria were chosen: no rain/irrigation occurred and daily solar irradiance (R_s) was over 80% of clear sky R_s. The DOY representing the sub-periods were BEG: 181-184, 186–189, 193–194; MID: 205–206, 208–209, 211, 213, 215, 217, 219, 222; END: 239–241, 244–245, 248–251, 254. For comparisons between sub-periods, an "average" day was computed for each sub-period by averaging data from the 10 days at each time step (15-min) during the 24-h period from midnight to midnight.

3. Results and discussion

3.1. Effect of soil water content measurement of G

In order to assess the effect of row direction on G and given the experimental setup constraints (no TDR measurements in the SE field), it was first mandatory to test the use of the HP sensors for the G computations. Values of θ_{TDR} vs. uncorrected and corrected θ_{HP} were examined in two ways. In the first, all TDR readings (10 locations, 2 depths, total of 20 sensors average, $\theta_{TDR\text{-}6\&2}$) were averaged, and in the second only the 10 TDRs deployed at 6 cm ($\theta_{TDR\text{-}6}$) were averaged. Since the HPs were inserted centered at a depth of 5 cm, the comparison with $\theta_{TDR\text{-}6}$ is considered reasonable. However, G is most accurately computed if the soil water content at both depths is accounted for, so a comparison of θ_{HP} with $\theta_{TDR\text{-}6\&2}$ was also conducted.

There was a distinct non-linear relationship between θ_{HP} and both $\theta_{TDR\text{-}6\&2}$ and $\theta_{TDR\text{-}6}$ (Fig. 3). This is likely due to: (i) the contributions of bulk electrical conductivity (BEC) and bound water to the apparent permittivity, both of which are temperature dependent; and (ii) the inability of the HP sensor to accurately measure BEC and temperature [17]. The "real" permittivity value output by the HP is simply the apparent permittivity corrected for the loss tangent, which itself is a function of the sensor's frequency of operation and the soil BEC. Since the HP does not accurately measure

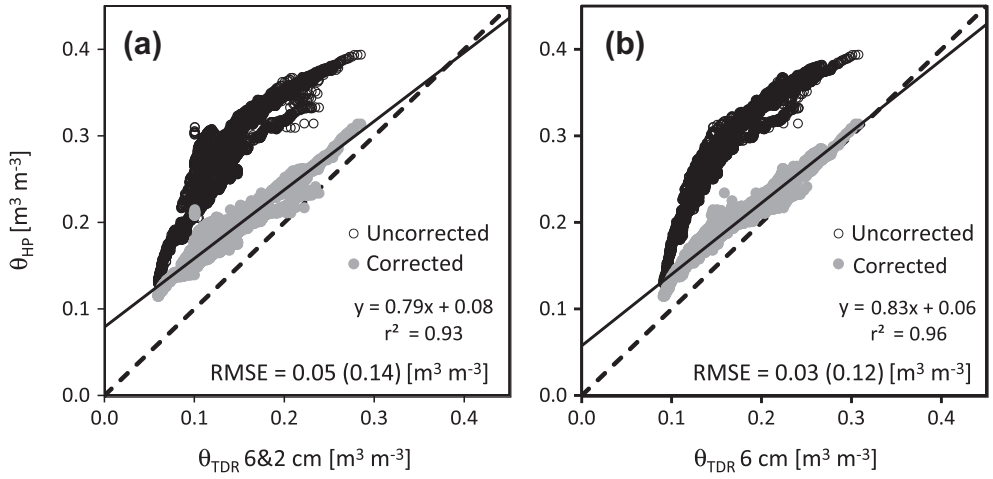

Fig. 3. Comparison of corrected and uncorrected Hydra Probe soil water content (θ_{HP}) vs. average TDR soil water content (θ_{TDR}) at depths of (a) both 6 and 2 cm ($\theta_{TDR\text{-}6\&2}$); and (b) only 6 cm ($\theta_{TDR\text{-}6}$).

the BEC [17], and there is no correction of the apparent permittivity for dielectric relaxation effects due to bound water (important in this soil), the estimated "real" permittivity value is unreliable. Correlation of θ_{TDR} with corrected θ_{HP} showed a significant improvement both in the slope and the linearity, with root mean square errors (RMSE) 3–4 times smaller. A complete correction would have to solve the dual problems of sensitivity of θ_{HP} to BEC and to bound water, both of which are temperature dependent but in different ways, as well as the problems with HP measurement of BEC and temperature. Those issues are beyond the scope of this paper. As expected, better agreement was found between $\theta_{TDR\text{-}6}$ and θ_{HP} compared with $\theta_{TDR\text{-}6\&2}$ vs. θ_{HP}, with a slope closer to unity, an intercept closer to 0, and a smaller RMSE of 0.03 vs. the value of 0.05 $m^3\ m^{-3}$ obtained for $\theta_{TDR\text{-}6\&2}$ vs. θ_{HP}.

Soil heat flux computed with corrected and uncorrected θ_{HP} (G_{HP}) was compared with G computed with $\theta_{TDR\text{-}6\&2}$ (G_{TDR}, Fig. 4). While uncorrected G_{HP} overestimated G by 27% (RMSE = 18 W m^{-2}) compared to G_{TDR}, corrected G_{HP} overestimated G by only 9% (RMSE = 12 W m^{-2}). This 9% overestimation may be a result of the HP data being from locations several meters from the heat flux plates and the existence of spatial variability in near surface soil moisture [36]. It is more likely, however, that the 9% over estimation resulted from the incomplete correction of HP water content data, which would have resulted in overestimated C_v and

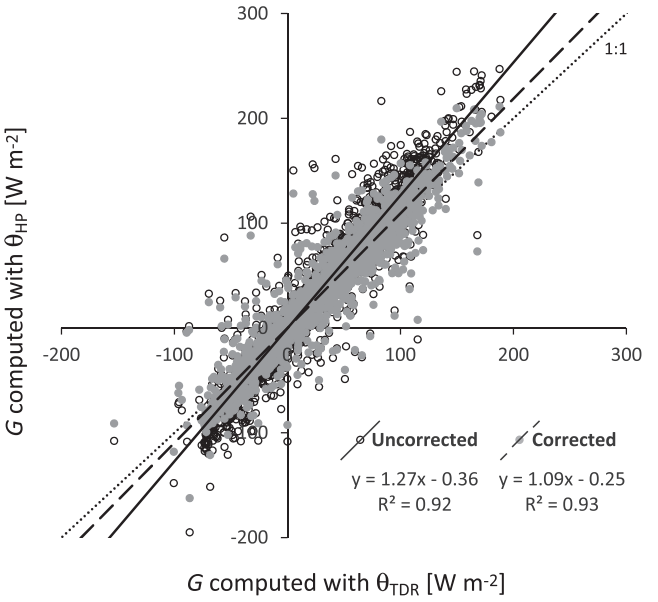

Fig. 4. Soil heat flux (G) computed with corrected and uncorrected Hydra Probe soil water content (θ_{HP}) compared to SHF computed with TDR soil water content (θ_{TDR}-6&2).

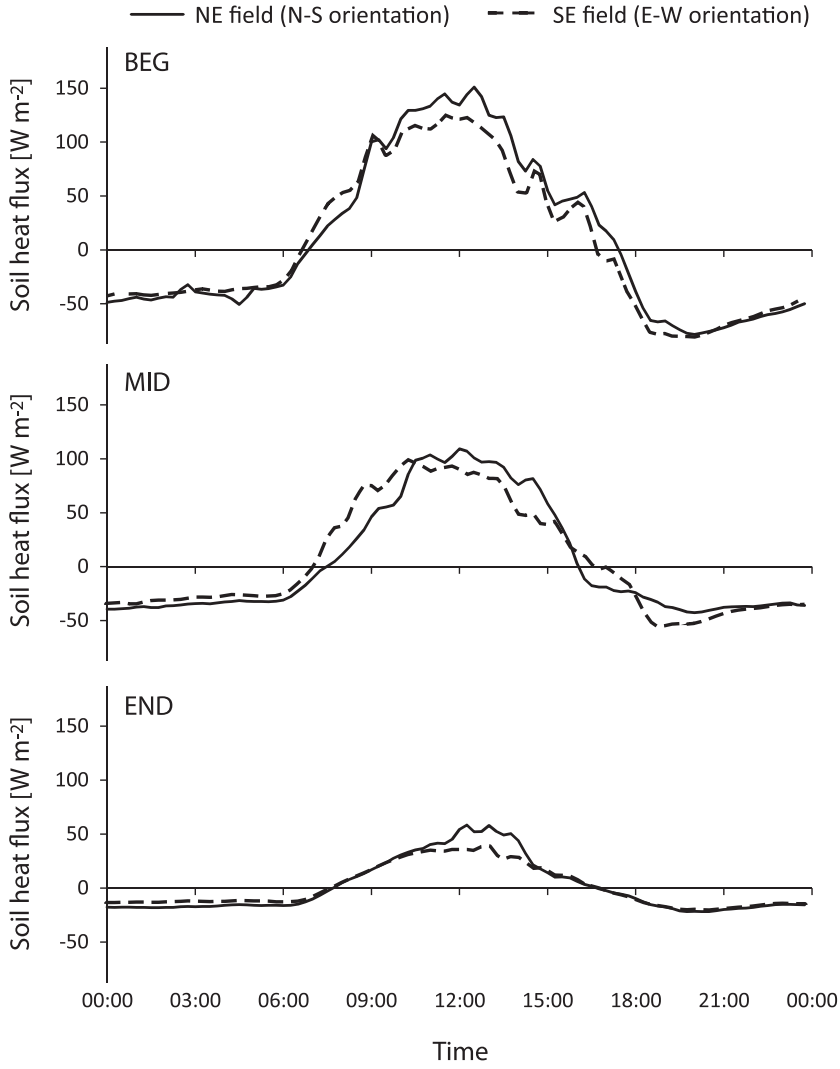

Fig. 5. Average soil heat flux in the NE and SE fields for the beginning (BEG), middle (MID) and end (END) sub-periods.

thus ΔG_s values. These results show the benefit of correcting the water content values from the HP sensors. Because we wish to contrast soil heat flux at the NE and SE sites and only θ_{HP} values were available at both sites, all subsequent analyses in this paper use G computed with corrected θ_{HP}.

3.2. Effect of row direction on the diurnal course of G

Differences in G can originate from various sources of variability in local thermal properties (e.g., soil moisture) as well as from the local incident radiation, the spatial variation of which is governed by shading of the canopy. It is hypothesized that local incident radiation influenced by shading is of prime importance. Diel patterns of (1/4)-hourly average values of G indicated recognizable differences between the N–S and E–W fields in all sub-periods (Fig. 5). Soil heat flux magnitudes tended to decrease with increasing f_c, with peaks of ~140, ~100, and ~50 W m^{-2} in the BEG, MID, and END sub-periods, respectively. In the BEG and MID sub-periods of the growing season, values of G immediately after sunrise and before 0900 CST were slightly larger in the SE field than values in the NE field, and values in both fields increased gradually, converging to relatively equal values at about 0900 CST. From 0900 CST to sunset, values of G in the NE field in the BEG sub-period tended to remain slightly larger than in the SE field. In the MID sub-period between sunrise and 1000 CST, values of G in the NE field were below those in the SE and *vice versa* from 1000 CST to sunset. For all sub-periods, there was a phase shift in the timing of maximum G with peak G occurring later in the NE compared to the SE field. In the END sub-period values of G were equal in both NE and SE except during the period from about 1100 to 1430 when G was ~30% greater in the NE field.

It was determined that the sun's diurnal course relative to the row direction was the main cause for these differences. This is illustrated by a plot of G at the five positions across the interrow ($G_{1\text{-}5}$) in both NE and SE fields (Fig. 6). At the beginning of the growing season (average f_c ~0.25, BEG sub-period) similar patterns of G were observed in both fields (Fig. 6a and b) for all positions except perhaps position 1 in the NE field. The different behavior of G at position 1 was likely due to intermittent shading and sunlit conditions immediately above the sensors, due to the presence of the emerging vegetation with incomplete cover along the rows.

Under partial vegetation cover (average f_c ~0.6, MID sub-period) a significant difference in the G patterns between the two row directions was observed (Fig. 6c and d). For the E–W row direction (SE field), variation in G across the five positions was observed, with largest differences between positions from 0900 to 1400 (Fig. 6c). These differences were governed by the fraction and position of sunlit/shaded soil. Overall, the magnitude in G_1 was relatively small, reflecting the fact that position 1 remained shaded throughout most of the day. The magnitude in G_2 was also

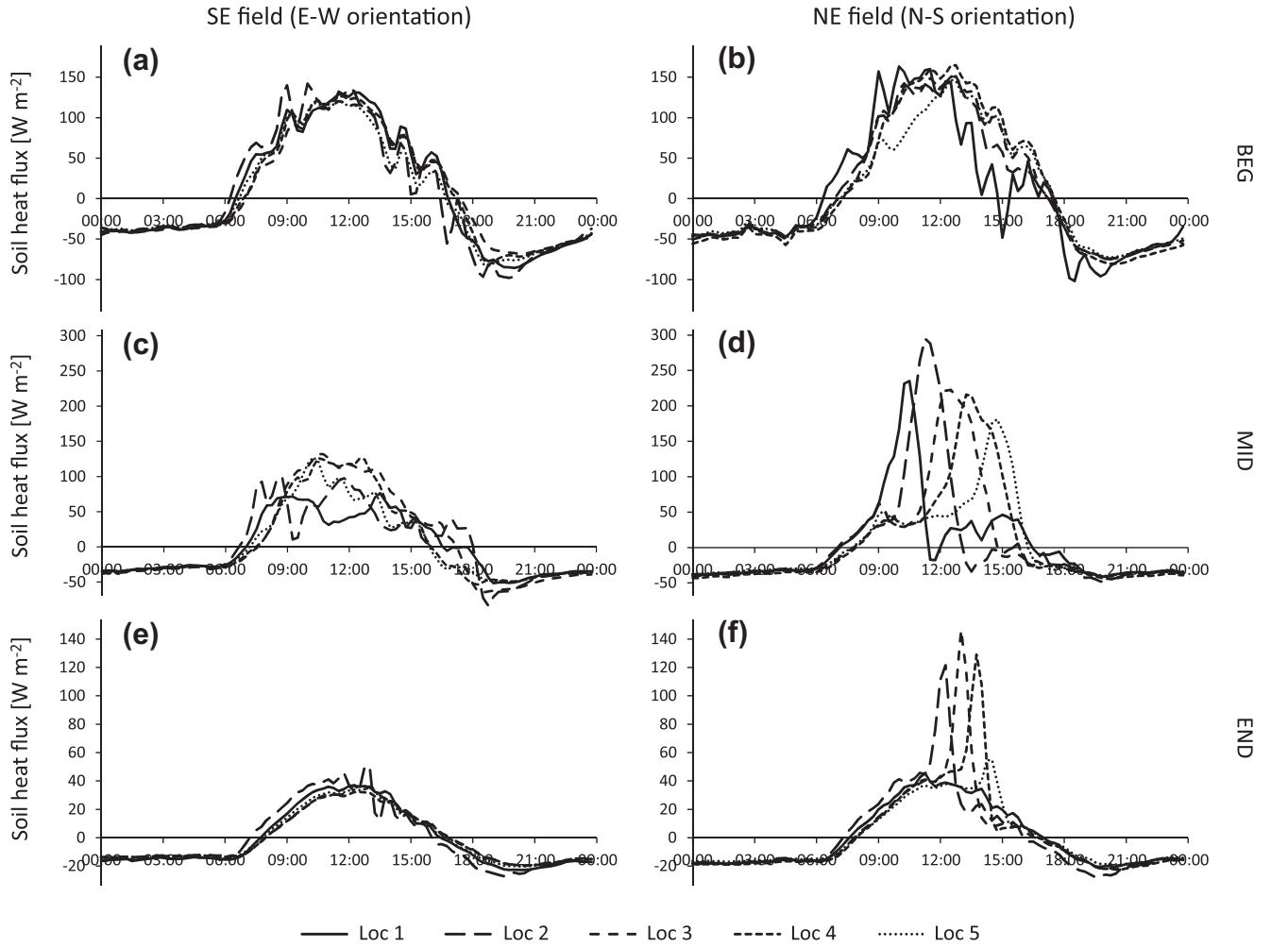

Fig. 6. Soil heat flux at 5 positions across the interrow. Data for each position is an average of that from the two sensors deployed in the same position relative to the row on one side. Data shown for the SE (panels a, c, and e) and NE (panels b, d, and f) fields for the beginning (BEG, panels a and b), middle (MID, panels c and d) and end (END, panels e and f) sub-periods.

quite small except for a short period in early morning, when a local peak in G_2 was observed, during which position 2 was exposed to direct solar radiation. Data for G_3 and G_4 yielded a typical sinusoidal curve, being exposed to direct radiation during the mid-day when the sun was highest in elevation. Although positioned at the same distance from the mid-row as position 1, G_5 data showed a different morning temporal response and pattern compared to G_1. This was due to the fact that positions 1 and 5 were on the south and to the north sides of the interrow, respectively, resulting in an opposite sunlit/shading effects as the sun transited from northeast to southeast.

Very different temporal patterns and G magnitudes for the five positions in the NE field were apparent in the MID sub-period (Fig. 6d). A slow increase in G after sunrise was common to all positions as long as all positions were shaded by the eastern row ($\varphi = 90 \pm 10°$, $\varphi > 50°$). Following the sun's azimuth and zenith angle positions over time, the first position exposed to direct solar radiation would be position 1 (furthest to the west) and ~2 h later, as the sun crossed to the south, position 1 was again shaded, this time by the western row next to which it was installed. This same temporal pattern with a significant spike in G was repeated for all positions, with a progressive ~2 h delay. After ~17:00, when $\varphi = 270 \pm 10°$ and $\varphi > 50°$ again, and until sunset (~2000), the entire interrow was again shaded, and G in all positions were small and similar in magnitude. The maximum values of G for all positions in the NE field significantly exceeded values observed for

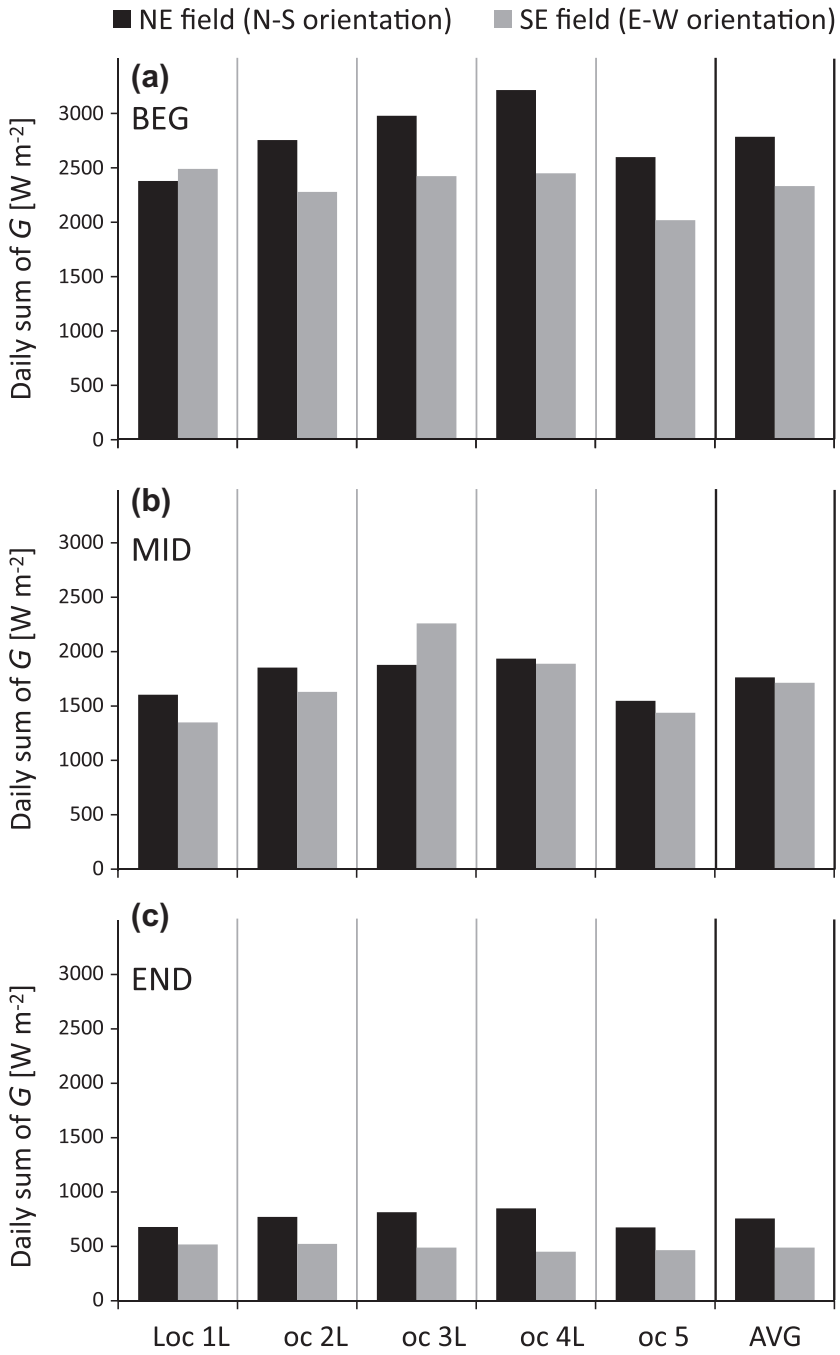

Fig. 7. Sums of daytime (sunrise to sunset) soil heat flux (SHF) at each position (Loc 1–5) and on average (AVG), for the NE and SE fields, in the beginning (BEG, panel a), middle (MID, panel b) and end (END, panel c) sub-periods.

all positions for the SE field; this must have to do with a different amount of direct radiation received by these two directions under mid cover fraction conditions.

In the END sub-period the rows were almost completely closed with f_c nearly 1. In the E–W direction field these conditions resulted in very little direct solar radiation reaching the soil throughout the interrow, and G had a smooth diurnal pattern, practically equal in all positions (Fig. 6e). In contrast, in the N–S direction, the remaining small gaps in canopy cover between the rows allowed for direct solar radiation to reach the center part of the interrow when the sun azimuth was mainly in the south. This caused the peaks observed for positions 2–4, similar to the patterns for the MID sub-period, but smaller in magnitude and shorter in duration.

If differences in G across the row were governed by local differences in thermal properties of the soil, they should have been detected over the night as well as throughout the day, but such nighttime differences were not observed. While large differences in G across the row were observed during the day, nocturnal G was similar across positions (Fig. 6). It is therefore concluded that the prime cause for the variability in G in a row crop setting is the sun's diurnal course relative to the direction of the rows.

3.3. Effect of row direction on daily sum of G

The effect of measurement position on daytime sum of G (ΣG) was examined for the three sub-periods (Fig. 7). In the BEG sub-period little difference in ΣG across positions 1–4 was observed in the SE field, with position 5 having a smaller value. In the NE field, ΣG was similar for positions 1 and 5, and was larger for the three more central positions with position 4 exhibiting the largest value. The magnitude of ΣG and the magnitude of change in ΣG were larger in the NE field compared to the SE field, with a difference between minimum and maximum ΣG of 836 vs. 472 W m^{-2}, respectively, for the NE and SE fields.

In the MID sub-period, ΣG_1 and ΣG_5 in both fields were smaller compared to positions 2–4, as positions 1 and 5 were already underneath the canopy and received less direct solar radiation. Variations in ΣG among positions were 388 and 910 W m^{-2} for the NE and SE fields, respectively. The larger variation in the SE field is opposite to the observed differences in the BEG sub-period. The smaller variation of ΣG in the NE field may be attributed to the spike-pattern that was common to all positions (Fig. 6). While larger short-term differences in G were observed between the positions in the NE relative to the SE fields, ΣG was more uniform across positions in the NE field.

In the END sub-period, minimal differences between positions were observed for ΣG in the SE field, with a magnitude of ~1/5 of that observed in the BEG sub-period, reflecting the fact that very little direct radiation was reaching to the soil at this stage. ΣG in all positions was larger in the NE field. While in the SE field ΣG was small (<500 W m^{-2}) and relatively constant across the row, in the NE field a pattern similar to the pattern observed for the previous two sub-periods was observed, with smaller magnitude for positions 1 and 5, and an increase towards the middle of the interrow. This reflects the fact that, in contrast to the E–W row direction, in the N-S row direction direct solar radiation did still reach the soil. Both the overall magnitudes of ΣG and the magnitude of positional changes in ΣG, however, were significantly smaller in this period compared to the BEG and MID sub-periods.

The mean ΣG_{AVG} in the NE was 19%, 3%, and 55% greater than in the SE field for the BEG, MID, and END sub-periods, respectively. The least difference in ΣG_{AVG} between the fields was observed in the MID sub-period, although differences in 15-min average G were greatest. Division of ΣG_{AVG} by daytime sum of R_n (Fig. 8) showed that the fraction G/R_n was reduced from ~0.12 to ~0.05 as the canopy developed, as expected. While in both the BEG and END sub-periods $\Sigma G_{AVG}/R_n$ was greater in the NE compared to the SE fields, in the MID sub-period $\Sigma G_{AVG}/R_n$ was greater in the SE field, albeit only by 0.3%. This reverse behavior (opposite to that observed in Fig. 7) was due to the difference in R_n between the two fields (see insert in Fig. 8), where R_n was greater in the NE field throughout the season. Note that an opposite result was observed by Steiner [39,40] who showed that for a 0.76-m row width planting of sorghum at Bushland, R_n was smaller in a N-S direction compared with E-W rows. The differences in R_n between the NE and SE fields always exceeded the measurement uncertainty and may reflect the effect of row direction on radiation interception, although cover fraction differences between the lysimeters and surrounding field complicates any definitive conclusions to be drawn from these measurements [37].

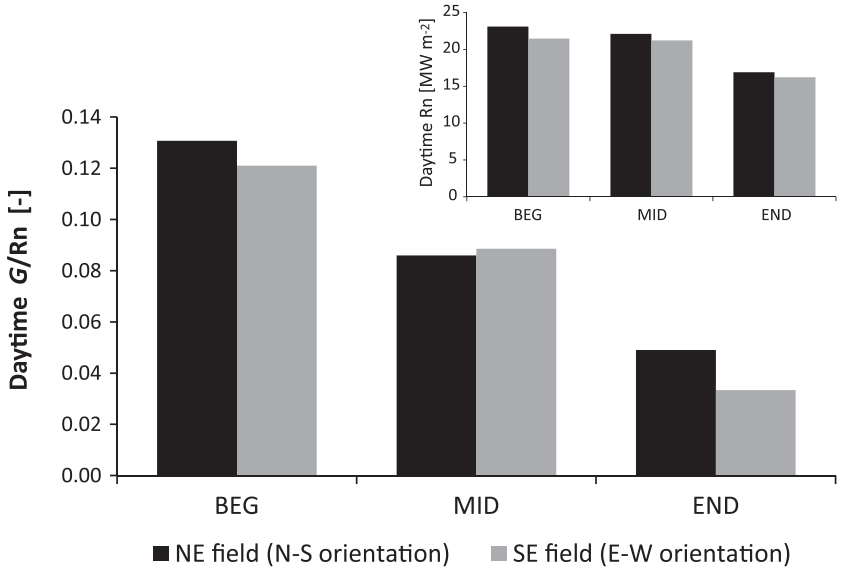

Fig. 8. Fraction of average daytime (sunrise to sunset) sum of soil heat flux from net radiation (R_n) in the NE and SE fields for the beginning (BEG), middle (MID) and end (END) sub-periods. In the insert: daytime sum of R_n in the NE and SE fields for the beginning (BEG), middle (MID) and end (END) sub-periods.

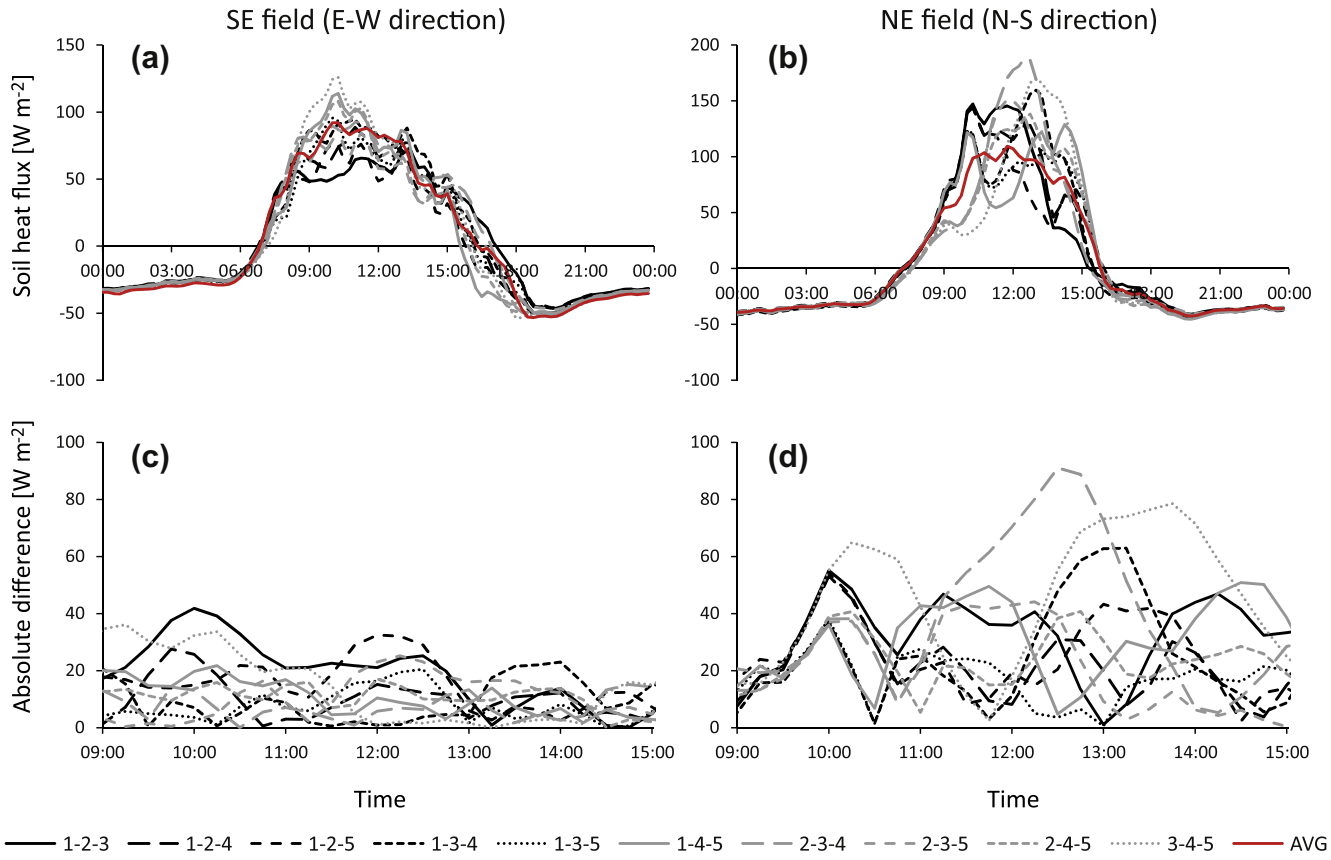

Fig. 9. Average *G* of all combinations of three replicates out of the five positions in the NE and SE fields (panels a and b, respectively), and differences between the 3-replicate averages and the 10-replicate average between 0900 and 1500 when errors were largest (panels c and d for the NE and SE fields), in the middle (MID) sub-period of the growing season.

The diurnal spatio-temporal variation in *G* observed in the NE field parallels that observed for evaporation from the soil surface as measured using microlyimseters by Agam et al. [41]. As with *G*, soil *E* peaked earlier in the day on the west side of the interrow and peaked later in the day on the east side of the interrow for N–S row direction. The positional effect on both *G* and soil evaporation was undoubtedly due to the west to east movement of the sunlit portion of the interrow during the day.

3.4. Implication for the number of replicates required

Based on previous studies it would seem difficult to determine the minimum number of sensors required for a reliable estimate of *G* for sparse canopies. Given the practical limitations to the number of sensors one can use to obtain a representative value within several meters of a flux tower [3], it is common practice in the flux tower community to use three replicates for estimating *G*. To test the number of replicates needed for the cotton row crop examined here, averages of *G*, computed using data from all possible combinations of three replicates out of the five sensor sets on one side of the site (locations 1–5 in Fig. 1), were compared with the 10-replicates average. This procedure was repeated for the five sensor sets (6–10 in Fig. 1) on the other side of the site. This resulted in 10 permutations for each set of 5-locations, for a total of 20 combinations of three replicates. In Fig. 9 only one set of 10 permutations is plotted since results from both sets were similar. Deviations/errors in *G* estimation were assessed for the MID subperiod, when positional effect on *G* was largest. Note the different patterns of *G* in Fig. 9a and b compared to Fig. 6c and d. While in Fig. 6 *G* was plotted for each position in the interrow (each the mean of data from two sensor sets) separately, in Fig. 9, 3-position averages were plotted, resulting in significantly different patterns, especially for the NE field.

In the SE field, with an E-W row direction, the diel course of all 3-replicate combinations was quite similar to the 10-location average. An average daytime error of 13 W m^{-2} was observed, with maximum error of 29 W m^{-2} on a short-term (15-min average) scale. The combination of locations 1, 3 and 5 resulted in a pattern most similar to the 10-location average, with average daytime errors as small as 7 W m^{-2} and maximum short-term error of 20 W m^{-2}. This implies that in an E-W row direction three replicates, strategically positioned, may marginally suffice to adequately represent *G* at micro-meteorological scales. This does not apply to the N-S row direction field, where average daytime error was 29 W m^{-2} and maximum short-term error of 62 W m^{-2}. The best 3-replicate combination in the NE field was also that of locations 1, 3, and 5, which yielded an average error of 17 W m^{-2} and a maximum short-term error of 38 W m^{-2}. Much more disconcerting than the error magnitude was the diurnal pattern. None of the combinations followed the 10-locations average diurnal course, due to the moving peaks at the 5 locations. It is concluded, therefore, that in a N–S row direction no 3-replicate combination is adequate to represent the patch-scale average *G* under partial canopy cover.

4. Conclusions

The main objective of this research was to study the effect of row direction on *G* magnitude and variability in an irrigated

semi-arid agricultural area. In addition, the effect of inaccurate water contents on computation of the storage term above the soil heat flux plate was assessed. Results indicate that errors in G may be large when using the capacitance method for measuring soil water content, even when a soil-specific calibration is performed. This is due to the sensitivity of capacitance sensors to bulk electrical conductivity and to bound water, both of which are temperature dependent. A full correction of capacitance sensors for these effects may not be possible for reasons explained by Evett et al. [42].

Given large differences in G across the row observed during the day, and the similar nocturnal G across locations, it is concluded that the prime cause for the variability in G in a row crop setting is the sun's diurnal course relative to the direction of the rows. This was reflected in the noticeable effect of row direction on G both in the diurnal course and when summing over daytime. Maximum differences were observed in the middle of the growing season under partial vegetation cover conditions ($f_c \sim 0.6$).

In the E–W direction field, means of data from any three replicates were found to adequately follow the pattern of G observed from the 10-location average. This implies that in an E–W row direction three replicates may marginally suffice to adequately represent G at micro-meteorological scales as long as they are properly placed to obtain adequate representation of the sunlit and shaded areas.

In the N-S row direction field all the 3-replicate combinations resulted in large errors and a different diurnal pattern compared to the 10-location average. It is concluded, therefore, that with N-S row direction, 3 replicates are not sufficient to adequately represent the patch scale average G no matter how those measurements are positioned across the interrow. This conclusion has important implications for situations where rows may curve as in circular rows under a center pivot irrigation system. Interestingly, for both row directions, the 3-replicate mean that was closest to the 10-location average was that computed for locations 1, 3, and 5.

References

[1] Clothier BE, Clawson KL, Pinter PJ, Moran MS, Reginato RJ, Jackson RD. Estimation of soil heat-flux from net-radiation during the growth of alfalfa. Agric For Meteorol 1986;37:319–29.

[2] Kustas WP, Daughtry CST. Estimation of the soil heat flux/net radiation ratio from spectral data. Agric For Meteorol 1990;49:205–23.

[3] Kustas WP, Prueger JH, Hatfield JL, Ramalingam K, Hipps LE. Variability in soil heat flux from a mesquite dune site. Agric For Meteorol 2000;103:249–64.

[4] Idso SB, Aase JK, Jackson RD. Net radiation-soil heat flux relations as influenced by soil water content variations. Bound-Layer Meteorol 1975;9:113–22.

[5] Heilman JL, McInnes KJ, Savage MJ, Gesch RW, Lascano RJ. Soil and canopy energy balances in a west Texas vineyard. Agric For Meteorol 1994;71:99–114.

[6] Ogee J, Lamaud E, Brunet Y, Berbigier P, Bonnefond JM. A long-term study of soil heat flux under a forest canopy. Agric For Meteorol 2001;106:173–86.

[7] Hsieh CI, Huang CW, Kiely G. Long-term estimation of soil heat flux by single layer soil temperature. Int J Biometeorol 2009;53:113–23.

[8] Sauer TJ, Horton R. Soil heat flux. In: Hatfield JL, Baker JM, editors. Micrometeorology in agricultural systems. American Society of Agronomy; 2005. p. 131–54.

[9] Anthoni PM, Law BE, Unsworth MH, Vong RJ. Variation of net radiation over heterogeneous surfaces: measurements and simulation in a juniper-sagebrush ecosystem. Agric For Meteorol 2000;102:275–86.

[10] Baldocchi DD, Law BE, Anthoni PM. On measuring and modeling energy fluxes above the floor of a homogeneous and heterogeneous conifer forest. Agric For Meteorol 2000;102:187–206.

[11] Mayocchi CL, Bristow KL. Soil surface heat-flux – some general questions and comments on measurements. Agric For Meteorol 1995;75:43–50.

[12] Fuchs M, Tanner CB. Calibration and field test of soil heat flux plates. Soil Sci Soc Am Proc 1968;32:326–8.

[13] Hanks RJ, Tanner CB. Calorimetric and flux meter measurements of soil heat flow. Soil Sci Soc Am Proc 1972;36:537–8.

[14] Brutsaert W. Evaporation into the atmosphere: theory, history and applications. Boston: D. Reidel; 1982.

[15] Topp GC, Davis JL, Annan AP. Electromagnetic determination of soil water content: Measurements in coaxial transmission lines. Water Resour Res 1980;16:574–82.

[16] Dalton FN, Herkelrath WN, Rawlins DS, Rhoades JD. Time-domain reflectometry – simultaneous measurement of soil-water content and electrical-conductivity with a single probe. Science 1984;224:989–90.

[17] Evett SR, Tolk JA, Howell TA. Time domain reflectometry laboratory calibration in travel time, bulk electrical conductivity, and effective frequency. Vadose Zone J 2005;4:1020–9.

[18] Dean TJ, Bell JP, Baty AJB. Soil-Moisture Measurement by an Improved Capacitance Technique. 1. Sensor Design and Performance. J Hydrol 1987;93:67–78.

[19] Paltineanu IC, Starr JL. Real-time soil water dynamics using multisensor capacitance probes: Laboratory calibration. Soil Sci Soc Am J 1997;61:1576–85.

[20] Evett SR, Schwartz RC. Discussion of "Soil Moisture Measurements: Comparison of Instrumentation Performances" by Ventura Francesca, Facini Osvaldo, Piana Stefano, and Rossi Pisa Paola February 2010, vol. 136(2), p. 81–9. DOI: 10.1061/(ASCE)0733-9437(2010)136:2(81). J Irrigat Drain Res 2011;137:466–8.

[21] Evett SR, Schwartz RC, Mazahreh N, Jitan M, Shaqir IM. Soil water sensors for irrigation scheduling: Can they deliver a management allowed depletion. Acta Horticult 2011;888:231–7.

[22] Evett SR, Schwartz SC, Tolk JA, Howel TA. Soil profile water content determination: Spatio-temporal variability of electromagnetic and neutron probe sensors in access tubes. Vadose Zone J 2009;8:926–41.

[23] Mazahrih NT, Katbeh-Bader N, Evett SR, Ayars JE, Trout TJ. Field calibration accuracy and utility of four down-hole water content sensors. Vadose Zone J 2008:992–1000.

[24] Stannard DI. Interpretation of surface flux measurements in heterogeneous terrain during the Monsoon '90 experiment. Water Resour Res 1994;30:1227–39.

[25] Ham JM, Kluitenberg GJ. Positional variation in the soil energy-balance beneath a row-crop canopy. Agric For Meteorol 1993;63:73–92.

[26] Shao C, Chen J, Li L, Xu W, Chen S, Gwen T. Spatial variability in soil heat flux at three Inner Mongolia steppe ecosystems. Agric For Meteorol 2008;148:1433–43.

[27] Malhi Y, McNaughton K, Von Randow C. Low frequency atmospheric transport and surface flux measurements. In Lee X, Massman W, Law B, editors. Handbook of micrometeorology, 2004. p. 101–18.

[28] Baldocchi D, Wilson K, Goldstein A, Falge E, Aubinet M, Berbigier P, et al. Energy balance closure at FLUXNET sites. Agric For Meteorol 2002;113:223–43.

[29] Kukharets VP, Nalbandyan HG, Foken T. Thermal interactions between the underlying surface and a nonstationary radiation flux. Izv Atmos Ocean Phys 2000;36:318–25.

[30] Liebethal C, Huwe B, Foken T. Sensitivity analysis for two ground heat flux calculation approaches. Agric For Meteorol 2005;132:253–62.

[31] Allen RG, Pereira LS, Howell TA, Jensen ME. Evapotranspiration information reporting: I. Factors governing measurement accuracy. Agric Water Manag 2011;98:899–920.

[32] Evett SR, Kustas WP, Gowda PH, Howell TA. Overview of the Bushland Evapotranspiration (ET) and Agricultural Remote sensing EXperiment 2008 (BEAREX08): A field experiment evaluating techniques quantifying ET at multiple scales. Adv. Water Resour 2012;50:4–19.

[33] Sauer TJ, Ochsner TE, Horton R. Soil heat flux plates: Heat flow distortion and thermal contact resistance. Agronomy J 2007;99:304–10.

[34] Evett SR, Heng LK. Conventional time domain reflectometry systems. In: Evett SR, Heng LK, Moutonnet P, Nguyen ML, editors. Field Estimation of Soil Water Content: A Practical Guide to Methods, Instrumentation, and Sensor Technology. Vienna, Austria: International Atomic Energy Agency; 2008. p. 55–72.

[35] Seyfried MS, Grant LE, Du E, Humes K. Dielectric loss and calibration of the hydra probe soil water sensor. Vadose Zone J 2005;4:1070–9.

[36] Cosh MH, Evett SR, McKee LG. Surface soil water content spatial organization within irrigated and non-irrigated agricultural fields. Adv. Water Resour 2012;50:55–61.

[37] Alfieri JG, Kustas WP, Prueger JH, Hipps LE, Evett SR, Basara JB, et al. On the discrepancy between eddy covariance and lysimetry-based turbulent flux measurements under strongly advective conditions. Adv. Water Resour 2012;50:62–78.

[38] Stevens Water Monitoring System I. The Hydra Probe Soil Sensor: Comprehensive Stevens Hydra Probe User's Manual. Beaverton, OR, 2007.

[39] Steiner JL. Dryland grain sorghum water use, light interception, and growth responses to planting geometry. Agronomy J 1986;78:720–6.

[40] Steiner JL. Radiation balance of dryland grain sorghum as affected by planting geometry. Agronomy J 1987;79:259–65.

[41] Agam N et al. Evaporative loss from irrigated interrows in a highly advective semi-arid agricultural area. Adv Water Resour 2012;50:20–30.

[42] Evett SR, Schwartz RC, Casanova JJ, Heng LK. Soil water sensing for water balance, ET and WUE. Agr Water Manage 2012;104:1–9.